frontiers in Materials

ORIGINAL RESEARCH
published: 08 January 2020
doi: 10.3389/fmats.2019.00330

# All-Inorganic Perovskite Solar Cells With Both High Open-Circuit Voltage and Stability

*Lei Zhang[1], Tianle Hu[2], Jinglei Li[3,4]*, Lin Zhang[3,4], Hongtao Li[5], Zhilun Lu[6] and Ge Wang[6]*

*[1] School of Microelectronics, Academy for Advanced Interdisciplinary Studies, Southern University of Science and Technology, Shenzhen, China, [2] Innovation Center of Computational Physics Methods and Software and State Key Laboratory for Superhard Materials, College of Physics, Jilin University, Changchun, China, [3] Electronic Materials Research Laboratory, Key Laboratory of Education Ministry, Xi'an Jiaotong University, Xi'an, China, [4] International Center for Dielectric Research, School of Electronic Science and Engineering, Xi'an Jiaotong University, Xi'an, China, [5] Shenzhen Institutes of Advanced Technology, Chinese Academy of Sciences, Shenzhen, China, [6] Department of Materials Science and Engineering, University of Sheffield, Sheffield, United Kingdom*

Metal halide perovskite solar cells based on all-inorganic $CsPbBr_3$ have attracted considerable attentions recently, due to their high open-circuit voltage and good stability. However, the fabrication of $CsPbBr_3$ film is limited by the poor solubility of cesium precursors in organic solvents by the one-step method. Here, we successfully fabricated $CsPbBr_3$ film solar cells by employing colloid nanocrystal. The effects of technique parameters, including purification times, anneal temperatures, and spin-coating times on film morphology, optical spectra, and device performance are investigated in detail. The highest power conversion efficiency of 4.57% has been achieved based on a large open-circuit voltage of 1.45 V and a large short-circuit current of 9.41 mA $cm^{-2}$. A large open-circuit voltage results from the reduced non-radiative energy loss channels and defect states while a large short-circuit current is related to the high conductivity induced by the removal of organic ligands with the increased nanocrystal electronic coupling. Furthermore, excellent stability in air is disclosed on the unencapsulated device suggesting the enormous potential for developing high open-circuit photovoltaic devices with high stability in future.

**Keywords: inorganic perovskite, solar cell, stability, open-circuit voltage, nanocrystals**

OPEN ACCESS

***Edited by:***
*Kalisadhan Mukherjee, Pandit Deendayal Petroleum University, India*

***Reviewed by:***
*Changrong Zhou, Guilin University of Technology, China*
*Kaixin Song, College of Electronics and Information, Hangzhou Dianzi University, China*

****Correspondence:***
*Jinglei Li*
*lijinglei@xjtu.edu.cn*

***Specialty section:***
*This article was submitted to Functional Ceramics, a section of the journal Frontiers in Materials*

***Received:*** *06 November 2019*
***Accepted:*** *03 December 2019*
***Published:*** *08 January 2020*

***Citation:***
*Zhang L, Hu T, Li J, Zhang L, Li H, Lu Z and Wang G (2020) All-Inorganic Perovskite Solar Cells With Both High Open-Circuit Voltage and Stability. Front. Mater. 6:330. doi: 10.3389/fmats.2019.00330*

## INTRODUCTION

The past few years have witnessed the significant development of organic-inorganic halide perovskite photovoltaics. The highest certified power conversion efficiency (PCE) of perovskite solar cells (PSCs) has reached up to 25.2% until now (NREL, 2019), which is close to that of the commercial polycrystalline silicon arising from high charge carrier mobility, long carrier diffusion length, and high light absorptivity across whole visible region (Green et al., 2014; Huang et al., 2017; Yang et al., 2018). Unfortunately, organic-inorganic halide perovskites suffer from intrinsicly thermal instability and easy-degradation under oxygen and water, which could be overcome by employing the all-inorganic halide perovskite $CsPbX_3$ (X=Cl, Br, I) without volatile organic components (Cho et al., 2018). It is worth mentioning that the stability of perovskite solar cells is determined by the stability of perovskite materials to some extent, so the performance degradation is unavoidable using unstable perovskite composition. Bulk $CsPbI_3$ with cubic structure has a small bandgap of 1.73 eV, which is ideal sunlight absorbing material. However, it undergoes immediate

phase transition from cubic to orthorhombic phase when exposed to ambient condition which is due to the orthorhombic yellow phase is thermodynamically preferred (Swarnkar et al., 2016; Sanehira et al., 2017; Zhang et al., 2017; Li B. et al., 2018; Wang et al., 2019). The large bandgap of $CsPbCl_3$ makes it impossible in photovoltaic applications. $CsPbBr_3$ has a direct gap of 2.36 eV, as well as high phase stability, thermal stability, and photo-stability. Although the overall PCE is limited by a relatively larger bandgap, $CsPbBr_3$ has been targeted as a potential material for stable high-voltage perovskite solar cells (Akkerman et al., 2016; Liang et al., 2016; Hoffman et al., 2017; Duan et al., 2018). More importantly, the all-inorganic PSCs using $CsSnBr_3$ QDs as interfacial decoration produce a maximized PCE of 10.60%, which is the highest reported PCE of $CsPbBr_3$ PSCs to date (Zhao et al., 2019). Compared with PSCs based on pure $CsPbBr_3$ nanocrystals (NCs), ion-doped or mixed PSCs have also attracted increased interests. $CsPbBrI_2$ has reasonable broad bandgap, and stable cubic phase at room temperature, with a continuously improved PCE (Sutton et al., 2016; Niezgoda et al., 2017; Zeng et al., 2018; Zhang J. et al., 2018). It was reported that $Cs_{0.91}Rb_{0.09}PbBr_3$ tailored solar cell achieved a high PCE of 9.86% resulted from the suppressed non-radiative losses and radiative recombination (Li Y. et al., 2018). The $CsPbI_{3-x}Br_x$ solar cell reported by Ye et al. achieved an open circuit voltage of 1.25 V and a highest PCE of 18.64% for all-inorganic PSCs. By inserting LiF in $SnO_2$ layer, the passivation of interface defects and optimized band alignement are achieved (Ye et al., 2019).

The fabrication technique has a significant impact on the film morphology and final device performance. Both one-step method and two-step method have been successfully employed to fabricate organic-inorganic halide PSCs with a high PCE exceeding 20% (Jeon et al., 2014; Seok et al., 2018). However, the solution-based deposition methods are difficult to directly adapt for $CsPbBr_3$ because of the low solubility of cesium precursors in commonly used solvents (Kulbak et al., 2015; Chang et al., 2016; Hoffman et al., 2017). Besides, both methods are sensitive to processing conditions because crystal quality, film morphology, and optoelectronic performance are controlled in the same optimization step (Akkerman et al., 2016). Perovskite NCs provide an option to solve the above problems, and the crystal structure, as well as the optical/electrical properties were summarized and discussed in detail (Deng et al., 2019). The perovskite NCs are synthesized at the high temperature to guarantee the excellent crystal quality. The unique luminous properties, including a high photoluminescence quantum yield (PLQY) and a narrow PL emission line width are related to the low defect density and reduced non-radiative recombination process (Song et al., 2015, 2016), which is beneficial to obtain PSC with a high PCE. Moreover, perovskite NCs with a large surface/volume ratio have been demonstrated to restrain the generation of yellow phase and improve air stability (Swarnkar et al., 2016; Cho et al., 2018). Despite these advantages, a series of post-treatment techniques including purification and anneal temperature need to be optimized to fabricate compact

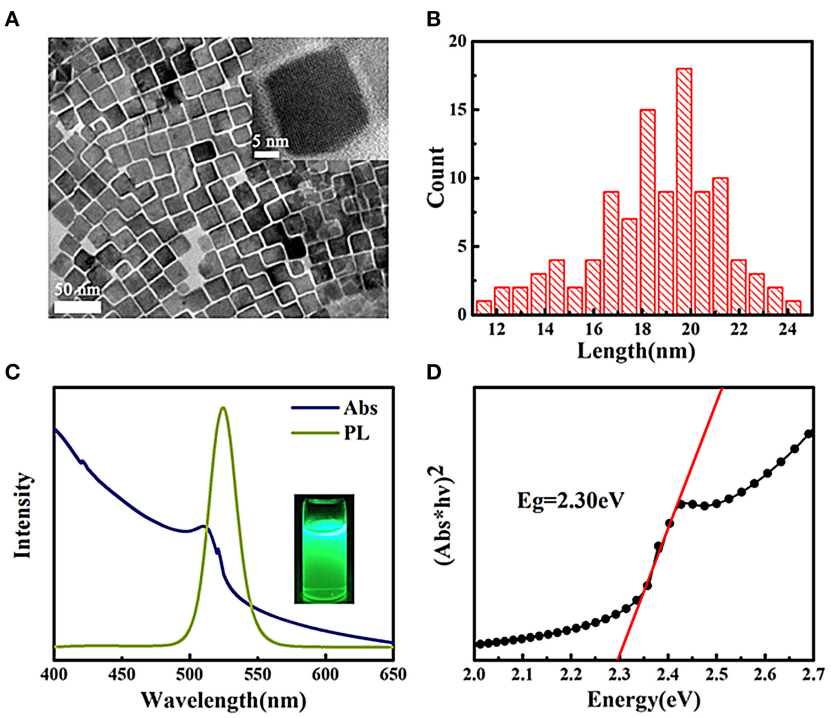


**FIGURE 1 | (A)** TEM images of $CsPbBr_3$ NCs, the inset is HRTEM images, **(B)** size distribution histogram, 100 particles were counted. **(C)** Optical absorption and PL spectra of $CsPbBr_3$ NCs solution, the inset is the photograph of NCs solution under UV excitation. **(D)** Tauc plot curve obtained from optical absorbance spectra.

and thickness-controllable perovskite NC films by layer-by-layer deposition method.

In this work, the morphology and optical spectra of $CsPbBr_3$ NCs are characterized. The purification and annealing temperature was effectively adjusted to obtain uniform and compact NC films with the purpose of improving conductivity. X-ray diffraction (XRD), PL spectra and transmission spectra were employed to study the influence of purification time on the crystal and the surface property of NC films. The impact of annealing temperature and film thickness on photovoltaic performance were investigated. Finally, the current density-voltage curves under different sweep rates and external quantum efficiency (EQE) were obtained on the device with the highest PCE, and its stability was also evaluated.

## EXPERIMENT SECTION

### Synthesis of $CsPbBr_3$ NCs

$CsPbBr_3$ NCs were synthetized using a hot injection method according to previous recipe. Briefly, Cs-oleate was synthetized by dissolving 0.1 g $Cs_2CO_3$ into 0.5 mL oleic acid and 3.7 mL 1-octadecene in a 100 mL round bottom 3-necked flask under $N_2$ flow at 120°C for 30 min. Pb-oleate was synthetized by blending 0.28 g $PbBr_2$, 2 mL oleylamine, 2 mL oleic acid, and 20 mL 1-octadecene in a round bottom flask under the same temperature. Then, 2 mL of Cs-oleate solution was promptly injected in Pb-oleate solution. The reaction flask was immediately transferred in an ice-water bath to complete the growth.

### Purification of $CsPbBr_3$ NCs

A typical purification procedure was as follows. Firstly, 2 mL hexane and 4 mL ethyl acetate were added into 2 mL $CsPbBr_3$ NCs crude solution. The precipitates were collected via centrifugation with a high-speed of 10,000 rpm for 5 min. Next, they were dispersed in 1 mL hexane and an equal amount of ethyl acetate for the second purification. The added solvent and antisolvent volumes reduced to 0.5 mL for the third purification. Finally, precipitates were dispersed in 0.2 mL mixed solvent hexane/octane (3:1 v/v).

### Fabrication of $CsPbBr_3$ NC Film Solar Cells

A 100-nm-thick $TiO_2$ layer was firstly deposited on a patterned FTO glass by spin-coating a Tetrabutyl titanate acidic solution at a speed of 3,500 rpm with a follow-on an air-annealing at a temperature of 400°C for 30 min. Then $CsPbBr_3$ NC solution was deposited on the $TiO_2$ layer by spin-coating at 1,500 rpm, and then the NC films were annealed in air at different temperatures for 15 min. The thickness of the film is increased by repeating the above step. Next, a mixed solution of

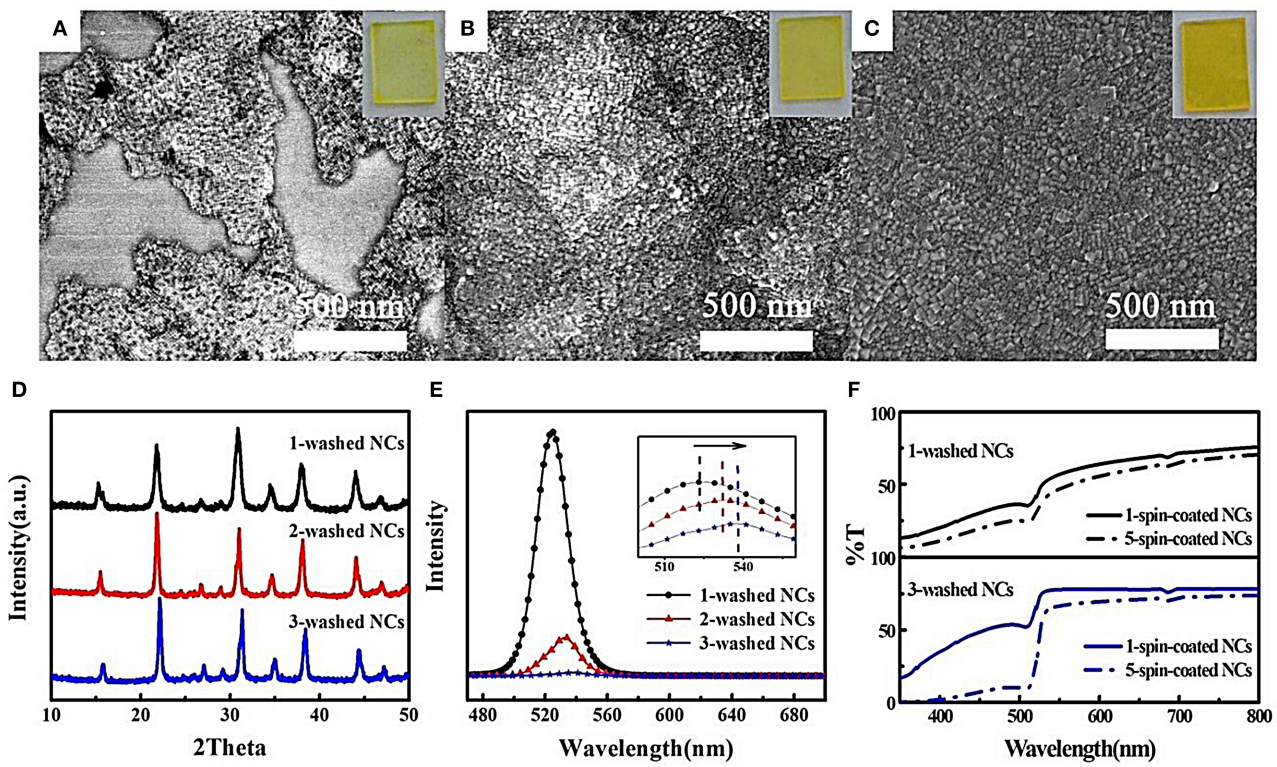


**FIGURE 2 |** The effects of purification times on morphology, crystal, and optical spectra of $CsPbBr_3$ NC films. SEM images of **(A)** 1 time **(B)** 2 times **(C)** 3 times washed NC films. The insets are corresponding photographs of NC films with different purification times. **(D)** XRD, **(E)** PL spectra, and **(F)** transmittance spectra of the NC films washed at different times. The inset in **(E)** is magnified PL spectra to show PL peak shift.

72.3 mg 2,2′,7,7′-tetrakis-(N,N-di-p-methoxyphenylamine)9,9′-spirobifluorene(Spiro-OMeTAD) in 1 mL chlorobenzene is spin-coated to form the hole-transporting layer at speed of 4,000 rpm for 60 s. At last, an Au electrode with a thick ness of 80 nm was coated by thermal evaporation.

## Characterization

Current density-voltage curves were characterized using a Keithley 2400 source meter under an AM1.5G solar simulator (SS-150, Sciencetech Inc.) in air. The EQE was measured by a certified incident photon-to-current conversion efficiency (IPCE) instrument (Beijing 7-Star Optical Instruments Co., Ltd.). The electrochemical impedance spectroscopy (EIS) was measured by an electrochemical workstation (CHI660D, Shanghai Chenhua Inc.) at a frequency range of 1 Hz−100 kHz and the amplitudes of 0–1.2 V. Microstructure was determined by a scanning electron microscope (SEM, Quanta 250, FEI) and a transmission electron micrograph (TEM, Arm2000F, Japan). Absorption and transmittance spectra were measured by a UV-Visible spectrophotometer (V-570, Jasco). PL spectra were carried out by a setup (Gilden Photonic Sens-9000) with a xenon lamp as the excitation source. XRD patterns were obtained by an X-ray diffraction spectrometer (D/max-2400, Rigaku, Japan).

## RESULTS AND DISCUSSION

The TEM images of $CsPbBr_3$ NCs are shown in **Figure 1A**. Uniform nanocubes are clearly observed with an interplanar spacing of 0.58 nm, which is consistent with the (200) plane in cubic phase (Protesescu et al., 2015; Zhang M. et al., 2018). **Figure 1B** shows a narrow size distribution with an average size of 19.47 nm for $CsPbBr_3$ NCs, which is in accordance with the narrow PL full width at the half maximum (FWHM) of 110 meV in **Figure 1C**. $CsPbBr_3$ has a Bohr exciton diameter of 7 nm and an exciton binding energy of 40 meV, which are responsible for a sharp excitonic absorption peak at 511 nm showed in **Figure 1C**. The PL peak at 525 nm indicates that no obvious quantum size effect is observed because the size of NCs is larger than Bohr exciton diameter, and a small Stokes shift of about 70 meV is obtained. $CsPbBr_3$ has a direct bandgap and the determined bandgap from the Tauc plot in **Figure 1D** is 2.30 eV, which is larger than that of bulk (2.25 eV) but a little smaller than that of nanosheet (2.32 eV) (Stoumpos et al., 2013; Song et al., 2016).

The colloid $CsPbBr_3$ perovskite NCs are stably dispersed in non-polar solvents because of the hydrophobic oleic acid and oleylamine ligands. In order to purify NCs, polar solvents are added as antisolvents to achieve centrifugation separation. Unfortunately, perovskite NCs are unstable (prone

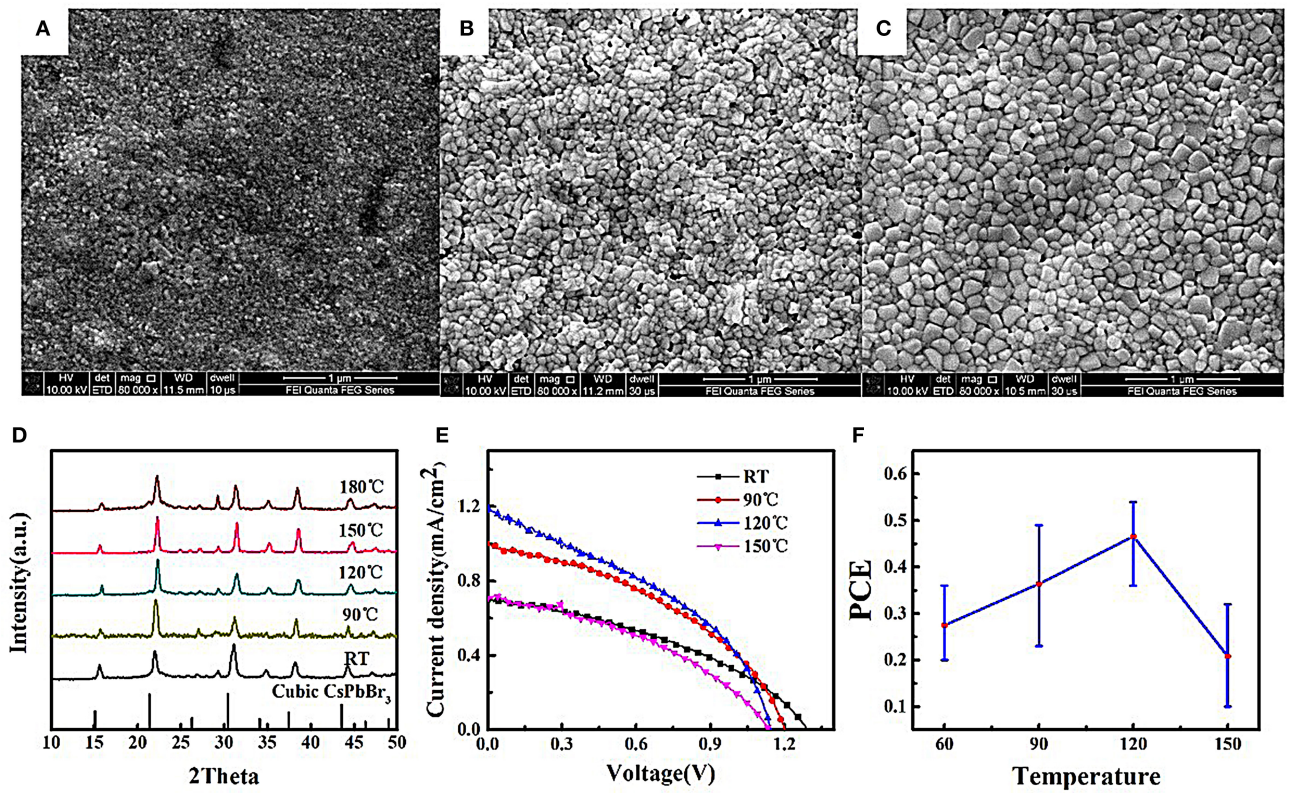


**FIGURE 3 |** The effects of annealing temperature on morphology and crystal of $CsPbBr_3$ NC films and solar cell performance. SEM images of **(A)** as-prepared **(B)** 90°C and **(C)** 180°C. **(D)** XRD patterns, **(E)** current density-voltage curves of NC film solar cells under AM 1.5 illumination, **(F)** the relationship between PCE and anneal temperatures.

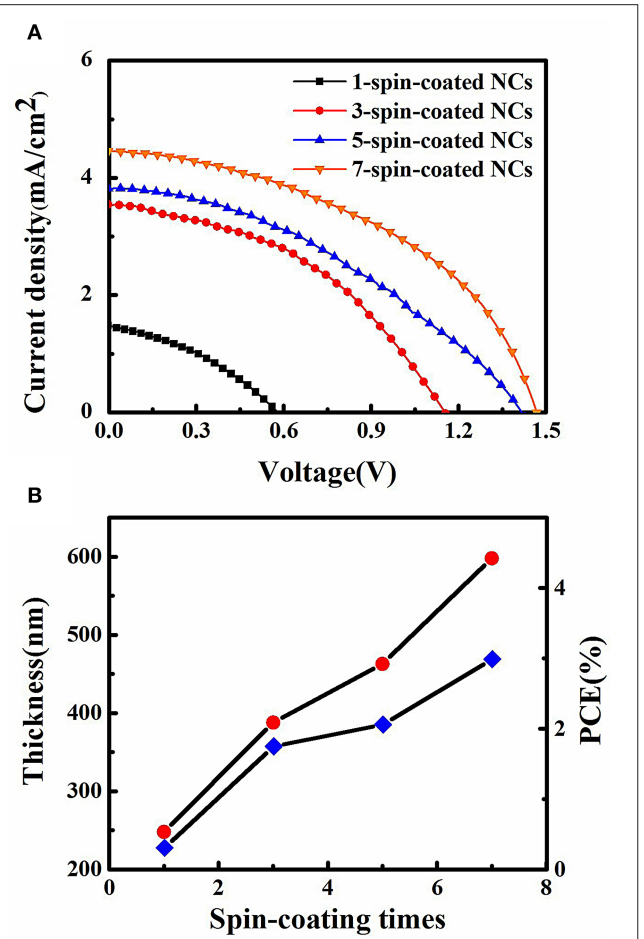


**FIGURE 4 | (A)** Current density-voltage curves of $CsPbBr_3$ NC film solar cells under AM 1.5 illumination, **(B)** The impact of spin-coating times on film thickness and PCE.

to dissolution) in polar solvents, resulting from their intrinsic ionic nature. As a result, antisolvent species and amounts, centrifugation speeds, and purification times are optimized to obtain well-dispersed NCs with high concentrations in order to meet the requirement of spin-coating NC films (Kim et al., 2015). Ethyl acetate was demonstrated to have the minimal side effect as an antisolvent (Li et al., 2016), but amounts and purification times are varied from batch to batch. The effects of purification times on the morphology of NC films are shown in **Figures 2A–C**. A large area of the uncovered substrate is observed for one-time-washed film, and NCs are unclear because of lots of residual organic ligands. Increased film coverage and dark yellow are obvious with the increase of purification times. For three-time-washed film, a high resolution of NCs suggests a high conductivity, and compact film is the prerequisite of reducing leakage current in solar cells. XRD patterns in **Figure 2D** show $CsPbBr_3$ NCs still maintain cubic phase after different purification times. The PL peak intensity is obviously decreased along with a slight red-shift of PL peak (**Figure 2E**), indicating an increased NCs electronic coupling led by the removal of organic ligands. Moreover, transmittance spectra are used to verify the film thickness, as given in **Figure 2F**. With the increase of spin-coating time, the film thickness is found to increase for 3-time-washed film than 1-time-washed film because NC films can be redissolved during the layer-by-layer spin-coating deposition resulting from residual organic species for 1-time-washed NCs.

**Figures 3A–C** exhibits the surface morphology images of three NC films annealed at different temperatures, showing increased $CsPbBr_3$ crystal sizes with increasing anneal temperature. The XRD patterns in **Figure 3D** show that $CsPbBr_3$ NC maintains the cubic phase even after high-temperature annealing, suggesting no phase change during air-annealing. **Figures 3E**,F shows anneal temperature-dependent photovoltaic performance, which is mainly caused by different $J_{SC}$. The maximum PCE obtained for NC films annealed at 120°C results from its largest $J_{SC}$, which is a result of increasing carrier mobility due to decreased amount of grain boundary, in accordance with Zeng et al.'s results (Zeng et al., 2018). Although temperature annealing is beneficial to increase grain size and improve carrier mobility, the $J_{SC}$ decreases with increasing temperature to 150°C. It is strange that increased grain size does not contribute to an improved conductivity. It may result from that the partial oxidization of surface can improve the contact resistance of grains. Therefore, an inert atmosphere annealing may be helpful to improve conductivity under the high-temperature annealing.

Another parameter spin-coating time has a significant effect on NC film thickness and final solar cell performance. The photovoltaic performance of $CsPbBr_3$ NC films is shown in **Figure 4A**. Both monotonically increased $V_{oc}$ and $J_{sc}$ are found with the increasing spin-coating times. The device using 1-spin-coated NC film failed because low film coverage leads to current leakage. The $V_{oc}$ of 1.45 V for 7-spin-coated NC film is quite close to the highest report of 1.5 V for perovskite solar cells (Akkerman et al., 2016). The $E_{loss}$ can be described by the equation: $E_{loss} = E_g - eV_{OC}$, and a small $E_{loss}$ of 0.85 eV is obtained, resulting from the reduced non-radiative energy loss channels and defect states (Zeng et al., 2018). The $J_{sc}$ of 4.5 mA $cm^{-2}$ is not high enough compared with the highest values of 5.6 mA $cm^{-2}$ for $CsPbBr_3$ NC film solar cell and 7.5 mA $cm^{-2}$ for $CsPbBr_3$ solar cell by one-step method (Akkerman et al., 2016; Liang et al., 2016), and low $J_{sc}$ is attributed to low NC film conductivity. The relationship among spin-coating times, film thickness and device performance are summarized in **Figure 4B** and a linearly increased film thickness are observed. The highest PCE is obtained from 7-spin-coated NC film with a thickness of 600 nm. The increased PCE with increasing spin-coating times is attributed to increased photo-generated excitons separation due to enhanced visible light absorption and reduced current leakage.

A typical $CsPbBr_3$ NC film solar cell structure is FTO/$TiO_2$/$CsPbBr_3$ NC film/Spiro-OMeTAD/Au, and the thickness of every layer can be seen in **Figure 5A**. The best-performing solar cell exhibits a high PCE of 4.57% in **Figure 5B**, and we compare reported all-inorganic perovskite solar cells in **Table 1**. The smaller $J_{SC}$ resulting from narrow visible light absorption is the reason for lower PCE compared with $CsPbI_3$ and $CsPbBrI_2$ solar cells, but their large bandgap contributes to

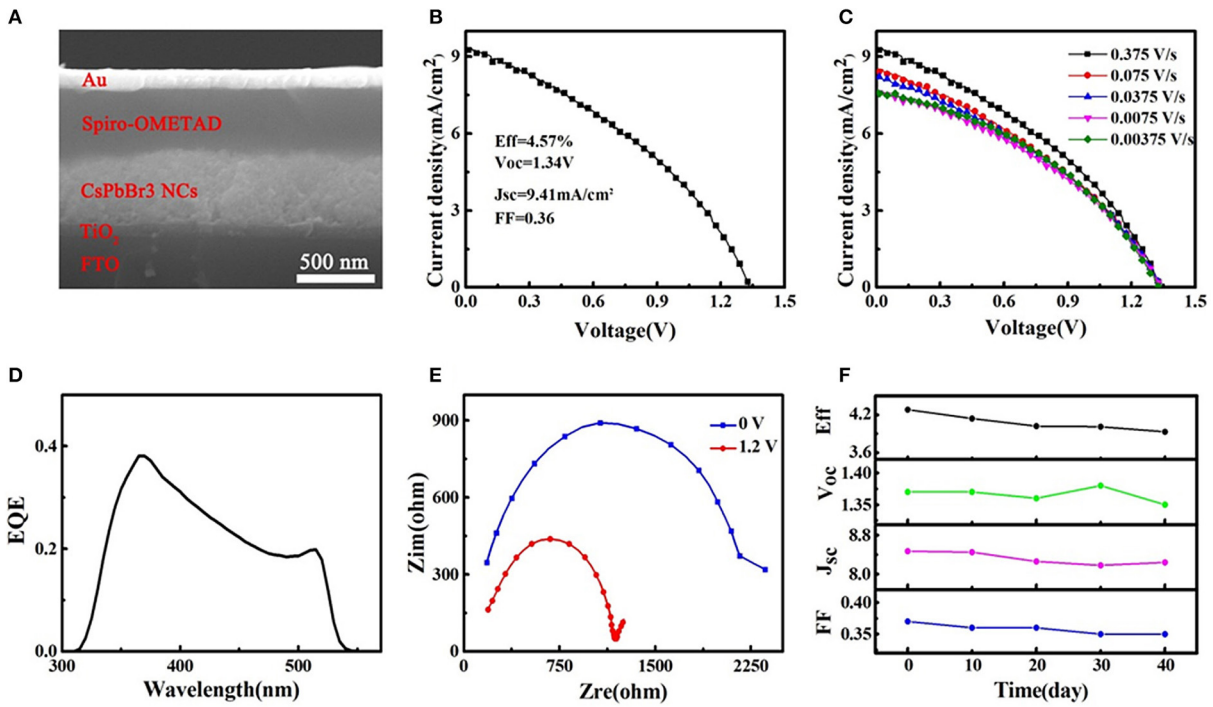


**FIGURE 5 |** $CsPbBr_3$ NC film photovoltaic device structure and performance. **(A)** Cross-sectional SEM images of device, **(B)** the current density-voltage curve of the best device under backward scan, **(C)** the current density-voltage curves obtained at different scan rate, **(D)** wavelength-dependent EQE curve. **(E)** Nyquist plots of device measured at different bias voltages under AM 1.5 illumination. **(F)** PCE stability of device without encapsulations stored in air.

**TABLE 1 |** Photovoltaic parameters for the all-inorganic perovskite solar cells.

| Perovskite | Film | $V_{oc}$ (V) | $E_{loss}$ (eV) | $J_{SC}$ (mA $cm^{-2}$) | FF (%) | PCE (%) | Reference |
|---|---|---|---|---|---|---|---|
| $CsPbI_3$ | NC film | 1.23 | 0.52 | 13.47 | 65 | 10.77 | Swarnkar et al., 2016 |
| $CsPbI_3$ | One-step film | 1.15 | 0.60 | 14.53 | 71 | 11.86 | Zhang et al., 2017 |
| $CsPbI_3$ | One-step film | 1.11 | 0.64 | 14.88 | 65 | 10.74 | Li B. et al., 2018 |
| $CsPbI_3$ | NC film | 1.20 | 0.55 | 14.37 | 78 | 13.4 | Sanehira et al., 2017 |
| $CsPbI_3$ | NC film | 1.11 | – | 19.62 | 0.74 | 16.1 | Wang et al., 2019 |
| $CsPbBr_3$ | NC film | 1.5 | 0.88 | 5.6 | 62 | 5.4 | Akkerman et al., 2016 |
| $CsPbBr_3$ | NC film | 1.42 | 0.96 | 7.01 | 53 | 5.6 | Hoffman et al., 2017 |
| $CsPbBr_3$ | two-step film | 1.24 | 1.14 | 7.4 | 73 | 6.7 | Liang et al., 2016 |
| $CsPbBr_3$ | two-step film | 1.32 | 0.98 | 6.91 | 54 | 4.92 | Kulbak et al., 2015 |
| $CsPbBr_3$ | NC film | 1.45 | 0.93 | 8.12 | 82.1 | 9.72 | Duan et al., 2018 |
| $CsPbBr_3$ | NC film | 1.61 | 0.77 | – | – | 10.6 | Zhao et al., 2019 |
| $Cs_{0.91}Rb_{0.09}PbBr_3$ | NC film | 1.55 | – | 7.73 | 82.2 | 9.86 | Li Y. et al., 2018 |
| $CsPbBrI_2$ | two-step film | 1.11 | 0.81 | 11.89 | 75 | 9.8 | Sutton et al., 2016 |
| $CsPbBrI_2$ | Two-step film | 1.08 | 0.84 | 12.96 | 66 | 9.22 | Niezgoda et al., 2017 |
| $CsPbBrI_2$ | NC film | 1.32 | 0.5 | 13.13 | 70 | 12.02 | Zeng et al., 2018 |
| $CsPbBrI_2$ | NC film | 1.19 | 0.73 | 12.93 | 80 | 12.39 | Zhang J. et al., 2018 |
| $CsPbI_{3-x}Br_x$ | NC film | 1.234 | – | 18.3 | 82.58 | 18.64 | Ye et al., 2019 |
| $CsPbBr_3$ | NC film | 1.34 | 0.96 | 9.41 | 36 | 4.57 | This work |

larger $V_{OC}$. We can find increased $J_{SC}$ with increased scan rate in **Figure 5C**, according to previous results. The EQE spectra of the device is shown in **Figure 5D**, and the cut-off wavelength is about 550 nm resulting from wide bandgap of $CsPbBr_3$, explaining its smaller $J_{SC}$ compared with $CsPbI_3$ and $MAPbI_3$ solar cells (Swarnkar et al., 2016; Sanehira et al., 2017; Zhang

et al., 2017; Li B. et al., 2018). The interfacial charge transfer process of device under illumination is revealed by the EIS spectra as given in **Figure 5E**. It is clearly observed decreased charge transfer resistance ($R_{ct}$) with the increase of applied bias voltage, which is resulted from the efficient extraction of more carriers. At the same time, the charge recombination resistance ($R_r$) is decreased by significantly enhancement of the free charge carriers in perovskite layer (Yang et al., 2015). The low $R_{ct}$ and $R_r$ under illumination illustrate the ideal contact interface between perovskite and transport layer. Finally, the unencapsulated device exhibits excellent stability in **Figure 5F**. It retains around 90% of initial PCE after 40 days of storage in air, and a reduced PCE is mainly caused by decreased $J_{SC}$, which is possibly attributed to the damage of the interface between perovskite and organic HTL. Therefore, the high air-stability contributes to solidifying $CsPbBr_3$ NC film solar cell as a kind of high-$V_{OC}$ and stable device.

## CONCLUSIONS

In summary, we have fabricated planar structure $CsPbBr_3$ NCs solar cells, and the average size of colloid $CsPbBr_3$ NC is 19.47 nm. The effects of purification times, anneal temperature and spin-coating times on morphology and crystal of $CsPbBr_3$ NC films were investigated. The compact and high conductivity NC films were prepared using a 3-time purification NC solution, and an increased NCs electronic coupling resulting from the removal of organic ligands was revealed by a slight red-shift of PL peak. We observed increased $CsPbBr_3$ crystal sizes with increasing annealing temperature, contributing to the increased solar cell PCE. Besides, we also found monotonically increased $V_{oc}$ and $J_{sc}$ with increasing spin-coating times due to increased film thickness. After the above parameters optimization, the best-performing solar cell with a high PCE of 4.57% was obtained, and the unencapsulated device exhibits great stability exceed 40 daysin air, illustrating the enormous potential of high-$V_{OC}$ $CsPbBr_3$ NC film solar cell.

## DATA AVAILABILITY STATEMENT

All datasets generated for this study are included in the article/**Supplementary Material**.

## AUTHOR CONTRIBUTIONS

JL conceived the idea, directed, and supervised the project. LeZ took part in the device fabrication and characterization. TH, LeZ, HL, LiZ, ZL, and GW analyzed the data. All authors contributed to discussions.

## FUNDING

We acknowledge the support from National Natural Science Foundation of China (Grant Nos. 51802182, 51972263, 51802142, 51572214, 61604122, and 51372196), China Postdoctoral Science Foundation (Grant No. 2019M660253), and 111 Program (Grant No. B14040). JL thanks the Fundamental Research Funds for the Central Universities (Grant No. sxjh012019011) and the Foundation of Shenzhen Science and Technology Innovation Committee (Grant Nos. JCYJ20180302174439113, JCYJ20180504170444967). The authors declare no competing financial interests.

## ACKNOWLEDGMENTS

Associate professor Zhi Yang helped prepared the paper. We thank him for his language editing.

## SUPPLEMENTARY MATERIAL

The Supplementary Material for this article can be found online at: https://www.frontiersin.org/articles/10.3389/fmats.2019.00330/full#supplementary-material

**Data Sheet 1 |** XRD pattern of $CsPbBr_3$ nanocrystals.

## REFERENCES

Akkerman, Q. A., Gandini, M., Di Stasio, F., Rastogi, P., Palazon, F., Bertoni, G., et al. (2016). Strongly emissive perovskite nanocrystal inks for high-voltage solar cells. *Nat. Energy* 2:16194. doi: 10.1038/nenergy.2016.194

Chang, X., Li, W., Zhu, L., Liu, H., Geng, H., Xiang, S., et al. (2016). Carbon-based $CsPbBr_3$ perovskite solar cells: all-ambient processes and high thermal stability. *ACS Appl. Mater. Interfaces* 8, 33649–33655. doi: 10.1021/acsami.6b11393

Cho, H., Kim, Y. H., Wolf, C., Lee, H. D., and Lee, T. W. (2018). Improving the stability of metal halide perovskite materials and light-emitting diodes. *Adv. Mater.* 30:1704587. doi: 10.1002/adma.201704587

Deng, J., Li, J., Yang, Z., and Wang, M. (2019). All-inorganic lead halide perovskites: a promising choice for photovoltaics and detectors. *J. Mater. Chem. C* 7, 12415–12440. doi: 10.1039/C9TC04164H

Duan, J., Zhao, Y., He, B., and Tang, Q. (2018). High-purity inorganic perovskite films for solar cells with 9.72% efficiency. *Angew. Chem.* 57, 3787–3791. doi: 10.1002/anie.201800019

Green, M. A., Anita, H. B., and Snaith, H. J. (2014). The emergence of perovskite solar cells. *Nat. Photonics* 8, 506–514. doi: 10.1038/nphoton.2014.134

Hoffman, J. B., Zaiats, G., Wappes, I., and Kamat, P. V. (2017). $CsPbBr_3$ solar cells: controlled film growth through layer-by-layer quantum dot deposition. *Chem. Mater.* 29, 9767–9774. doi: 10.1021/acs.chemmater.7b03751

Huang, J., Yuan, Y., Shao, Y., and Yan, Y. (2017). Understanding the physical properties of hybrid perovskites for photovoltaic applications. *Nat. Rev. Mater.* 2:17042. doi: 10.1038/natrevmats.2017.42

Jeon, N. J., Noh, J. H., Kim, Y. C., Yang, W. S., Ryu, S., and Seok, S. I. (2014). Solvent engineering for high-performance inorganic–organic hybrid perovskite solar cells. *Nat. Mater.* 13, 897–903. doi: 10.1038/nmat4014

Kim, Y., Yassitepe, E., Voznyy, O., Comin, R., Walters, G., Gong, X., et al. (2015). Efficient luminescence from perovskite quantum dot solids. *ACS Appl. Mater. Interfaces* 7, 25007–250313. doi: 10.1021/acsami.5b09084

Kulbak, M., Cahen, D., and Hodes, G. (2015). How important is the organic part of lead halide perovskite photovoltaic cells? Efficient $CsPbBr_3$ cells. *J. Phys. Chem. Lett.* 6, 2452–2456. doi: 10.1021/acs.jpclett.5b00968

Li, B., Zhang, Y., Fu, L., Yu, T., Zhou, S., Zhang, L., et al. (2018). Surface passivation engineering strategy to fully-inorganic cubic $CsPbI_3$ perovskites for high-performance solar cells. *Nat. Commun.* 9:1076. doi: 10.1038/s41467-018-03169-0

Li, J., Xu, L., Wang, T., Song, J., Chen, J., Xue, J., et al. (2016). 50-Fold EQE improvement up to 6.27% of solution-processed all-inorganic perovskite $CsPbBr_3$ QLEDs via surface ligand density control. *Adv. Mater.* 28:4861. doi: 10.1002/adma.201603885

Li, Y., Duan, J., Yuan, H., Zhao, Y., He, B., and Tang, Q. (2018). Lattice modulation of alkali metal cations doped $Cs_{1-x}R_xPbBr_3$ halides for inorganic perovskite solar cells. *Sol. RRL*. 2:1800164. doi: 10.1002/solr.201800164

Liang, J., Wang, C., Wang, Y., Xu, Z., Lu, Z., Ma, Y., et al. (2016). All-inorganic perovskite solar cells. *J. Am. Chem. Soc.* 138, 15829–15832. doi: 10.1021/jacs.6b10227

Niezgoda, J. S., Foley, B. J., Chen, A. Z., and Choi, J. J. (2017). Improved charge collection in highlyefficient CsPbBrI2 solar cells with light-induced dealloying. *ACS Energy Lett.* 2, 1043–1049. doi: 10.1021/acsenergylett.7b00258

NREL (2019). *Best Research-Cell Efficiencies*. https://www.nrel.gov/pv/assets/pdfs/best-reserch-cell-efficiencies.20190802.pdf.

Protesescu, L., Yakunin, S., Bodnarchuk, M. I., Krieg, F., Caputo, R., Hendon, C. H., et al. (2015). Nanocrystals of cesium lead halide perovskites ($CsPbX_3$, X = Cl, Br, and I): novel optoelectronic materials showing bright emission with wide color gamut. *Nano Lett.* 15, 3692–3696. doi: 10.1021/nl5048779

Sanehira, E. M., Marshall, A. R., Christians, J. A., Harvey, S. P., Ciesielski, P. N., Wheeler, L. M., et al. (2017). Enhanced mobility $CsPbI_3$ quantum dot arrays for record-efficiency, high-voltage photovoltaic cells. *Sci. Adv.* 3:4204. doi: 10.1126/sciadv.aao4204

Seok, S. I., Grätzel, M., and Park, N. G. (2018). Methodologies toward highly efficient perovskite solar cells. *Small* 14:1704177. doi: 10.1002/smll.201704177

Song, J., Li, J., Li, X., Xu, L., Dong, Y., and Zeng, H. (2015). Quantum dot light-emitting diodes based on inorganic perovskite cesium lead halides ($CsPbX_3$). *Adv. Mater.* 27, 7162–7167. doi: 10.1002/adma.201502567

Song, J., Xu, L., Li, J., Xue, J., Dong, Y., Li, X., et al. (2016). Monolayer and few-layer all-inorganic perovskites as a new family of two-dimensional semiconductors for printable optoelectronic devices. *Adv. Mater.* 28, 4861–4869. doi: 10.1002/adma.201600225

Stoumpos, C. C., Malliakas, C. D., Peters, J. A., Liu, Z., Sebastian, M., Im, J., et al. (2013). Crystal growth of the perovskite semiconductor $CsPbBr_3$: a new material for high-energy radiation detection. *Cryst. Growth Des.* 13, 2722–2727. doi: 10.1021/cg400645t

Sutton, R. J., Eperon, G. E., Miranda, L., Parrott, E. S, Kamino, B. A., Patel, J. B., et al. (2016). Bandgap-tunable cesium lead halide perovskites with high thermal stability for efficient solar cells. *Adv. Energy Mater.* 6:1502458. doi: 10.1002/aenm.201502458

Swarnkar, A., Marshall, A. R., Sanehira, E. M., Chernomordik, B., Moore, D. T., Christians, J. A. et al. (2016). Quantum dot–induced phase stabilization of α-$CsPbI_3$ perovskite for high-efficiency photovoltaics. *Science* 354, 92–95. doi: 10.1126/science.aag2700

Wang, Y., Dar, M. I., Zhang, T. Y., Kan, M. W., Li, Y., Zhang, L. J., et al. (2019). Thermodynamically stabilized β-$CsPbI_3$-based perovskite solar cells with efficiencies >18%. *Science* 365, 591–595. doi: 10.1126/science.aav8680

Yang, Z., Wang, M., Ding, J., Sun, Z., Li, L., Huang, J., et al. (2015). Semi-transparent ZnO-CuI/CuSCN photodiode detector with narrow-band UV photoresponse. *ACS Appl. Mater. Interfaces* 7, 21235–24244. doi: 10.1021/acsami.5b05222

Yang, Z., Wang, M., Qiu, H., Yao, X., Lao, X., Xu, S., et al. (2018). Engineering the exciton dissociation in quantum-confined 2D $CsPbBr_3$ nanosheet films. *Adv. Funct. Mater.* 28:1705908. doi: 10.1002/adfm.201705908

Ye, Q. F., Zhao, Y., Mu, S. Q., Ma, F., Gao, F., Chu, Z. M., et al. (2019). Cesium lead inorganic solar cell with efficiency beyond 18% via reduced charge recombination. *Adv. Mater.* 31:1905143. doi: 10.1002/adma.201905143

Zeng, Q., Zhang, X., Feng, X., Lu, S., Chen, Z., Yong, X., et al. (2018). Polymer-passivated inorganic cesium lead mixed-halide perovskites for stable and efficient solar cells with high open-circuit voltage over 1.3 V. *Adv. Mater.* 30:1705393. doi: 10.1002/adma.201705393

Zhang, J., Bai, D., Jin, Z., Bian, H., Wang, K., Sun, J., et al. (2018). 3D-2D-0D interface profiling for record efficiency all-inorganic $CsPbBrI_2$ perovskite solar cells with superior stability. *Adv. Energy Mater.* 30:1703246. doi: 10.1002/aenm.201703246

Zhang, M., Wang, M., Yang, Z., Li, J., and Qiu, H. (2018). Preparation of all-inorganic perovskite quantum dots-polymer composite for white LEDs application. *J. Alloys Compd.* 748, 537–545. doi: 10.1016/j.jallcom.2018.03.179

Zhang, T., Dar, M. I., Li, G., Xu, F., Guo, N., Grätzel, M., et al. (2017). Bication lead iodide 2D perovskite component to stabilize inorganic α-$CsPbI_3$ perovskite phase for high-efficiency solar cells. *Sci. Adv.* 3:1700841. doi: 10.1126/sciadv.1700841

Zhao, Y., Duan, J., Yuan, H., Wang, Y., Yang, X., He, B., and Tang, Q. (2019). Using $SnO_2$ QDs and $CsMBr_3$ (M=Sn, Bi, Cu) QDs as charge-transporting materials for 10.6%-efficiency all-inorganic $CsPbBr_3$ perovskite solar cells with an ultrahigh open-circuit voltage of 1.610 V. *Sol. RRL* 3:1800284. doi: 10.1002/solr.201800284

**Conflict of Interest:** The authors declare that the research was conducted in the absence of any commercial or financial relationships that could be construed as a potential conflict of interest.